Delamination Growth under Mixed Mode I - Mode II Fatigue Loading in Polymer Composite

KADLEC Martin[1,a] and ŠEDEK Jakub[1,b]

[1]VZLU – Czech Aerospace Research Centre, Beranových 130, 199 05 Prague – Letňany, Czech Republic

[a]kadlec@vzlu.cz, [b]sedek@vzlu.cz

Abstract. The characterization of material parameters on mixed mode bending (MMB) specimens was needed for modelling of crack growth in the composite air inlet of new L-39 NG jet trainer. The paper describes methods and results of the delamination growth in a carbon fibre-reinforced polymer composite under mixed mode I (opening) – mode II (shear) quasi-static and fatigue loading. This article summarizes the results of 15 quasi-static and 3 fatigue specimens tested in 3 different mode mixtures – 25%, 50% and 80%. The fracture toughness was increasing with the increasing mode mixture. The scatter of values was increasing with the mode II preference. The curves of crack growth rate vs. strain energy release rate were obtained and fitted by a regression model considering the mode mixtures. The dependence of crack growth law parameters according to Paris equation on the mode mixtures was non-linear. Thus, unique material characteristics needed for modelling were obtained.

Introduction

Fatigue damage accumulation and crack growth in metallic and composite materials are critical for the structural integrity evaluation. In recent years, composite materials have been widely used for structural components, especially in the field of aerospace engineering.

The delamination between plies of the laminate is one of the most important damage mechanisms. The air inlet has curved shape and so the mixed mode I (opening) and mode II (shear) loading can be expected when the delamination occur. The mode III contribution in delamination growth is typically quite small for composite structures due to the constraints of adjacent plies [1] and therefore it was not considered [1].

Several analytical models have been proposed and experimentally evaluated [1-3]. The results showed general non-linear relation of parameters used for the crack growth description in the form of Paris law. The FE-modelling employing cohesive zone models is also appropriate. It was concluded that only with implementing a cyclic damage variable in the cohesive interface element the experimentally observed crack growth and stiffness degradation can be captured properly [4].

The aim of this work is to determine the input data for the modelling of damage evolution in the composite air inlets of the newly emerging aircraft L-39NG. The data will be used to evaluate acoustic fatigue properties of the inlet using finite element (FE) analyses.

Methods

Material. Carbon fibre-reinforced composite Hexply AGP 193PW/8552S RC40 with the 16 layers lay-up of $[45/0]_{4S}$ was manufactured and MMB specimens were extracted with dimensions of 185 x 25 x 3.3 mm. During manufacturing, a non-adhesive plastic foil sheet was embedded into the plate near the edge during manufacturing to the neutral axis to initiate the delamination growth between the 8th and 9th layer. A pair of aluminium alloy blocks with dimensions of 25 mm x 20 mm x 10 mm was bonded using R 21 MP-2 instant cyanoacrylate adhesive to the end of each specimen on the side with non-adhesive insert. These blocks are used to apply the load to the specimens. Then a white paint marker was coated on the specimen edges to reveal the crack front during loading. Both edges of the specimen were marked using black lines with the spacing of 25 mm.

A series of 10 specimens was used for quasi-static testing and 5 specimens were used for fatigue testing. The specimens were divided to cover pure Mode I and three different mode mixtures – G_{II}/G = 25%, 55% and 85% (shear component of G / total strain energy release rate G).

Test setup. Tests were performed on non-aged specimens at room temperature, ambient atmospheric pressure and ambient relative humidity. A special fixture designed according to ASTM D6671M-06 [5] standard was employed (Fig. 1). Three test rig configurations were used to achieve different loading modes. Double cantilever beam (DCB) method was used to induce pure mode I. A pair of video cameras with the resolution of 2048 x 1536 pixels was focused onto the edges to cover the area between supports.
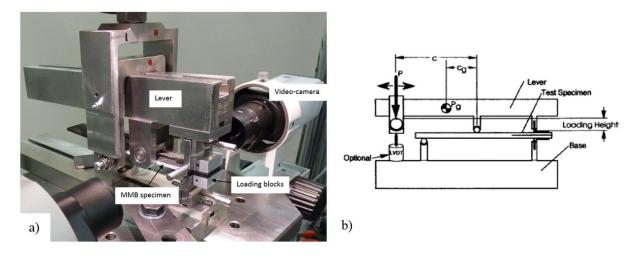

Fig.1 a) Mixed-mode bending test set-up and b) schematic of the mixed mode bending [5]

The ASTM D6671M-06 standard was used for evaluation of the quasi-static test and the maximum strain energy release rate G in the cycle was determined. The load was performed with a constant speed of 1 mm/min until the crack propagated by at least 25 mm. During loading the crack propagation was monitored using the cameras at 12.5 frames per second.

The values of G_I and G_{II} corresponding to the crack length a were calculated from Eq. 1 and Eq. 2, where parameters of fixture L, c, c_g were set.

$$G_I = \frac{12[P(3c - L) + P_g(3c_g - L)]^2}{16b^2h^3L^2E_{1f}}(a + \chi h)^2$$

(1)

$$G_{\mathrm{II}} = \frac{9[P(c + L) + P_g\,(c_g + L)]^2}{16b^2h^3L^2E_{1f}}\,(a + 0.42\chi h)^2 \tag{2}$$

Variables E_{1f}, χ and Γ were calculated according to Eq. 3 - 7, where $E_{11} = 68\,000$ MPa, $E_{22} = 68\,000$ MPa and $G_{13} = 4\,000$ MPa. The parameter m_{cal} in Eq. 6 was obtained from a metal specimen calibration. P denotes the force, b is the specimen width and h is the specimen thickness.

$$E_{1f} = \frac{8(a_o + \chi h)^3\,(3c - L)^2 + [6(a_o + 0.42\chi h)^3 + 4L^3]\,(c + L)^2}{16L^2bh^3\left(\dfrac{1}{m} - C_{\mathrm{sys}}\right)} \tag{3}$$

$$\chi \equiv \sqrt{\frac{E_{11}}{11G_{13}}\left\{3 - 2\left(\frac{\Gamma}{1+\Gamma}\right)^2\right\}}, \qquad \Gamma \equiv 1.18\frac{\sqrt{E_{11}E_{22}}}{G_{13}} \tag{4, 5}$$

$$C_{\mathrm{sys}} = \frac{1}{m_{cal}} - C_{cal}, \qquad C_{cal} = \frac{2L\,(c + L)^2}{E_{cal}b_{cal}t^3} \tag{6, 7}$$

The relations between the components G_{I} and G_{II} and the total value of G are as follows (Eq. 8, and Eq. 9.):

$$G = G_{\mathrm{I}} + G_{\mathrm{II}} \qquad \frac{G_{\mathrm{II}}}{G} = \frac{G_{\mathrm{II}}}{G_{\mathrm{I}} + G_{\mathrm{II}}} \tag{8, 9}$$

For fatigue, the test was driven by displacement amplitude $\delta_{max} = 6$ mm and $\delta_{min} = 0.6$ mm with frequency of 5 Hz. Currently there is no standard for fatigue delamination during mixed-mode loading and therefore the quasi-static based ASTM D6671M-06 standard was used for the evaluation. The maximum fracture toughness in the cycle was determined according to Eq. 1- 9. The crack propagation during the following loading was monitored using video cameras.

The crack propagation length for the individual specimens used for the compliance calibration was determined from the snapshots of the video recording. The length was measured from the picture using an in-house software with a virtual gauge. The author invented VZLU modified compliance calibration (VMCC) that was used for data reduction and fitted better to the experimental results than classic MCC method. The constants, A_1 and k from Eq. 10, were determined for individual specimens using a least-square fit applied to the plot of the optically observed delamination lengths (a/h) squared versus the cube root of the corresponding compliance C. For each specimen, the constants were used specifically for one specimen. The relationship between the compliance and the delamination length for the VMCC solution is:

$$(a/h)^2 = A_1 \cdot C^{\frac{1}{3}} + k, \tag{10}$$

where the compliance C is δ_{max}/P_{max} and h is the specimen thickness. The fitted constants A1 and k were used for the crack length a determination for each cycle using Eq. 10, based on the continuous P_{max} recorded from the test machine. For this purpose, the displacement δ_{max} was constant during loading.

The specimen was cycled until unstable crack growth occurred and the crack reached the middle support making the crack front not visible. Polynomial method was used to calculate the crack growth rate $\Delta a/\Delta N$. The method calculated $\Delta a/\Delta N$ by fitting a second-order polynomial to each set of 29 successive data points. The polynomial was used to calculate the value at the midpoint of the 29-point dataset.

The values of $(G_I)_{max}$ and $(G_{II})_{max}$ corresponding to the crack growth rate were calculated from Eq. 2 – Eq. 10.

FEM modelling. Performed static tests were evaluated using finite element approach utilizing cohesive zone model (CZM) implemented in ABAQUS 2017 software. In the analysis, the implicit solver ABAQUS/standard was used. Shell FE model consisted from 4 node thin shell elements with reduced integration scheme (S4R ABAQUS element type). Shell element included 3 through-thickness integration points. Characteristic FEM mesh size was 2 mm.

Model was symmetrically supported like in the three-point bending test. Loading was realized through kinematic coupling of loading points (Fig. 2). Nonlinearity due to displacement is taken into account. The loading was prescribed in displacement in the direction perpendicular to the specimen´s flat plane in the initial position. Two parts of the model were connected in the mid-plane by cohesive interaction. A nonlinear constitutive law represented the response of the material at the interface between plies. The linear-elastic softening behaviour was used in the analysis.
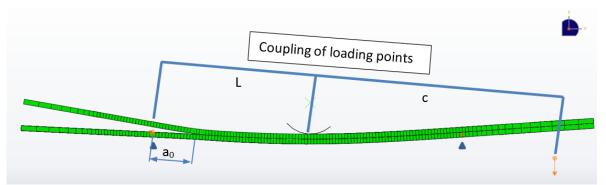

Fig.2 Finite element mesh boundary conditions and loading concept

In order to define the interfacial behaviour with a linear softening cohesive law, the initial stiffness K_i, critical values of driving force (delamination fracture toughness) G_{iC} in modes I, II and III and interlaminar strengths τ_i^0 in directions n, s and t are required. The values of listed parameters were used as follows: $K_i = 1.10^6$ N/mm³, $\tau_n^0 = 10$ N/mm², $\tau_s^0 = 20$ N/mm², $\tau_t^0 = 20$ N/mm², $G_{IC} = 650$ J/m², $G_{IIC} = 2300$ J/m², $G_{IIIC} = 2300$ J/m².

Quadratic traction relationship is used for combination of cohesive strengths and tractions in the form of Eq. 11. If the relation equals 1, the softening in connection begins.

$$\left(\frac{\langle \tau_n \rangle}{\tau_n^0}\right)^2 + \left(\frac{\langle \tau_s \rangle}{\tau_s^0}\right)^2 + \left(\frac{\langle \tau_t \rangle}{\tau_t^0}\right)^2 \tag{11}$$

Results

For quasi-static testing, the individual values of the fracture toughness showed exponential increase of fracture toughness (Fig. 3). The scatter of values was increasing with the G_{II} mode prevailing.
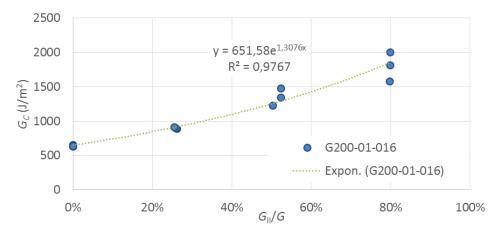
Fig.3 Total mixed-mode fracture toughness; experimental data and fitted exponential curve

For fatigue testing, the plots of the crack growth rate $v = \Delta a/\Delta N$ vs. $(G_I)_{max}$ were generated for all the fatigue specimens (Fig. 4). The curves are wavy which is caused by the carbon fabric structure that locally affects the crack growth rate [6]. It is clear that as mode II contribution increased (or mode I contribution decreased) the data moved consistently to the left (i.e. crack growth rate increasing with increasing mode II component of loading). This suggests that the mode II component has a significant influence on the crack growth rate.

These curves were used for generating the coefficients of the crack growth rate described by Eq. 12 in the form similar to Paris law for individual specimens.

$$\frac{\Delta a}{\Delta N} = A\left(G_i\right)_{max}^{\ r} \tag{12}$$

Fig. 5a shows the linear relation of coefficient log A with mode mix ratio. The coefficient A is increasing with higher mixture. Fig. 5b presents Paris law exponent polynomial relation with mode mix ratio where the exponent is decreasing with higher mode II component. Tab. 1 presents the values of fitted constants of the Paris law for individual mode mixtures.
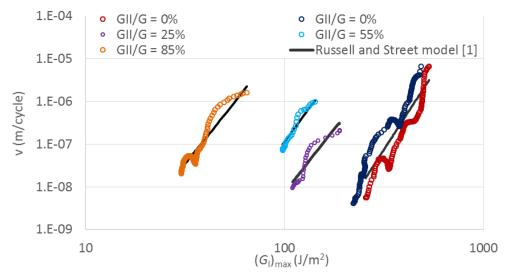

Fig.4 Crack grow rate data; experimental data and Russell and Street model fit [1]
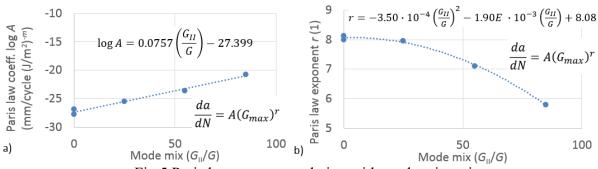
Fig.5 Paris law exponent relation with mode mix ratio

Tab. 1 Coefficients for Paris law at different mode-mixtures

Sample ID	Actual G_{II}/G	Paris law log A	Paris law r
009	0 %	-26.8677	8.002
006	0 %	-27.8142	8.134
014	24 - 28 %	-25.4931	7.957
016	53 - 55 %	-23.5969	7.112
010	83 - 85 %	-20.7375	5.796

Finally, all data were filtered and fitted by the Russell and Street analytical model (Fig. 4) obtained from the article [1], nevertheless other more recent models can be found [2, 3]. The model with 4 constants (A_I, A_{II}, r_I, r_{II}) is presented by Eq. (13). G_i denotes to maximum strain energy release rate in the cycle and ΔG_i to the range of G in the cycle. G_{ic} is fracture toughness.

$$\frac{da}{dN} = \left(\frac{G_I}{G_I + G_{II}}A_I + \frac{G_{II}}{G_I + G_{II}}A_{II}\right)\left(\frac{\Delta G_I}{G_{Ic}} + \frac{\Delta G_{II}}{G_{IIc}}\right)^{\left(\frac{G_I}{G_I+G_{II}}r_I + \frac{G_{II}}{G_I+G_{II}}r_{II}\right)} \tag{13}$$

The mode mixture is slightly changing during the crack growth as the fixture setup is fixed. Actual mode mixture range where the crack growth rate and the coefficients were evaluated is stated in Tab. 2.

Tab. 2 Coefficients for fatigue crack growth at different mode-mixtures determined by Eq. 12 fitting based on total energy release rates components of ΔG.

	A_I	A_{II}	r_I	r_{II}
Russell and Street model [1]	2.813E-05	4.976E-03	7.209	4.839

A finite element numerical simulation of quasi-static tests utilizing cohesive zone modelling was also evaluated. The analysis was performed for three values of G_{II}/G: 26, 54, and 80%. The results are presented in Fig. 6 together with only one representative experimental result for each G_{II}/G ratio (dashed lines).
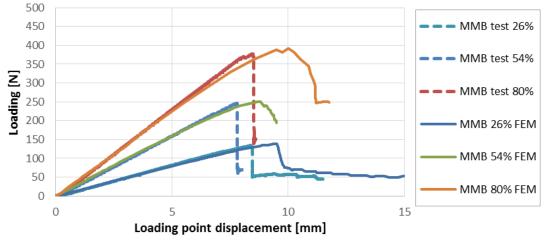
Fig.6 Load-displacement curves; FE analysis and representative experimental data

The initial stiffness is in good correlation with experimental data. Before the maximum load-carrying capacity the softening is present. The effect is more severe with G_{II}/G ratio increase. The maximum level of loading corresponds with the maximum test load, but displacement is greater in the FE analysis. The loss of load-carrying capacity is sharp in the case of experiment, but FE analysis shows gradual load decrease. It is also more severe with increase of G_{II}/G ratio. This response can be caused by gradual development of cohesive zone before crack advance; especially in mode II.

Conclusions

A method for fatigue crack growth evaluation under mixed mode I/II was established. The curves of crack growth rate vs. strain energy release rate were obtained and fitted by the analytical regression model considering the mode mixtures. In the FE-analysis, the cohesive zone modelling technique was used to represent the cohesive behaviour of interlaminar interface. The comparison of experimental data and computed load-displacement curves shows initial corresponding development, but slow crack advance in comparison with the experimental rapid crack growth. The experiment provides unique composite material data that can be sparsely found in the literature.

Acknowledgment

References

[1] N. Blanco, E.K. Gamstedt, L.E. Asp, J. Costa, Mixed-mode delamination growth in carbon–fibre composite laminates under cyclic loading, Int. J. Solids Struct. 41 (2004) 4219–4235.

[2] L. Zhao, et al., A novel interpretation of fatigue delamination growth behavior in CFRP multidirectional laminates, Compos. Sci. Tech. 133 (2016) 79-88.

[3] Y. Liu, C. Zhang, A critical plane-based model for mixed-mode delamination growth rate prediction under fatigue cyclic loadings, Compos. Part B. 139 (2018), 185-194.

[4] P. Naghipour, M. Bartsch, H. Voggenreiter, Simulation and experimental validation of mixed mode delamination in multidirectional CF/PEEK laminates under fatigue loading, Int. J. Solids Struct. 48 (2011), 1070-1081.

[5] ASTM Standard D6671M-06, Mixed Mode I-Mode II Interlaminar Fracture Toughness of Unidirectional Fiber Reinforced Polymer Matrix Composites, ASTM International, West Conshohocken, PA, 2006.

[6] M. Kadlec, L. Nováková, I. Mlch, L. Guadagno, Fatigue delamination of a carbon fabric/epoxy laminate with carbon nanotubes, Compos. Sci. Tech. 131 (2016) 32-39.